Evolution of quantum superpositions in open environments: Quantum trajectories, jumps, and localization in phase space

B. M. Garraway and P. L. Knight
Optics Section, The Blackett Laboratory, Imperial College, Prince Consort Road, London SW7 2BZ, United Kingdom
(Received 29 April 1994)

The decay of coherence when a quantum system interacts with a much larger environment is usually described by a master equation for the system reduced density matrix and emphasizes the evolution of an entire ensemble. We consider two methods that have been developed recently to simulate the evolution of single realizations. Quantum-state diffusion involves both *diffusion,* where the individual quantum trajectory fluctuates through a Wiener process deriving from the environment, and *localization* to a coherent state, an eigenstate of the relevant Lindblad operator describing the coupling of the system to the environment. We demonstrate the localization process for different initial states and utilize the Wigner function to depict this localization in phase space. We concentrate on quantum states that can be expressed as a superposition of appropriate coherent states. For an initial superposition of two coherent states (a Schrödinger "cat"), one of the two components will dominate the evolution. For initial Fock states, which can be described as a continuous superposition of coherent states on a ring, localization takes place when one coherent state is selected from that ring where each component has nearly the same energy as the original Fock state. We also consider the localization from a nonclassical squeezed ground state, which can be expressed as a superposition of coherent states along a *line* in phase space. The second simulation method considered is the state vector Monte Carlo, or "quantum jump," approach, which relates to the direct counting of decay quanta. In the case of an initial Schrödinger "cat," we find that when no quantum is detected the "cat" shrinks, but when a quantum *is* detected, the Schrödinger "cat" "jumps" from one type of "cat" to another with different internal phase. For an initial squeezed state we show how quantum jumps lead to individual realizations which are superpositions of *two* squeezed states.

PACS number(s): 42.50.Lc, 42.50.Dv

I. INTRODUCTION

Closed quantum systems evolving entirely through reversible Hermitian dynamics, are frequently employed in quantum dynamics, with the Jaynes-Cummings model of a single two-level atom interacting with a single quantum field mode being perhaps the best known example [1]. In such idealizations, subsystems become entangled and coherences created. In reality, no quantum system can ever be entirely isolated from its environment and its dynamics need to be supplemented to recognize the irreversible decay of energy and coherences characteristic of open systems [2]. A method which is widely adopted to describe such behavior is the master equation for the reduced density operator (having traced out the degrees of freedom of the larger environment) with the system-environment coupling treated in the Born-Markov approximation [3]. This method describes the evolution of an *ensemble* of realizations of the quantum system and shows that coherences (especially those characterizing macroscopic superpositions) decay much faster than the system energy [4–6]. This ensemble approach is well suited for problems such as those involving many atoms interacting with a radiation field. But it does not easily address the question of how an individual member of an ensemble evolves in a dissipative environment, even though this issue is accessible to experiment. For example, the quantum jumps in the fluorescence of a single three-level ion undergoing intermittent shelving in a metastable state [7,8] are well known. Similarly, quantum jumps in the photon excitation number of a single mode of a high-Q cavity have been studied theoretically [9,10] and experimentally [11]. Recently, methods to describe the evolution of single quantum systems interacting with an open environment have been developed for their intrinsic interest [8,12–27] and for practical computational reasons even when an ensemble is of primary interest [28–34].

In this paper we address the question of how a single realization of a superposition of radiation field states evolves in a dissipative environment. That is, we examine the evolution of prepared quantum superpositions *conditioned* by measurements we are able to make on the decay products of the dissipation, with the record of such conditioned measurements being particular to that realization. The evolution of such a superposition will of course depend on the precise measurement scheme adopted: for radiation fields one may imagine quadrature measurements of field variables as one such scheme or direct photon counting as another. All hinge ultimately on the counting of quanta. The state vector Monte Carlo method [12,13] has been developed to simulate the evolution of a single realization conditioned by the observation of decay quanta and centers on quantum jumps reflecting the information gained from such observations. It involves a continuous evolution which is interrupted by

 ©1994 The American Physical Society

"instantaneous" jumps as the state vector is conditioned by information gained from the register of counts. The other method commonly adopted involves both a quantum-state *diffusion* [15], where the individual quantum trajectory fluctuates through a Wiener process deriving from the environment, and *localization* to a coherent state [19], an eigenstate of the relevant Lindblad operator R describing the coupling of the system to the environment [35]. For example, in one-photon decay R is the annihilation operator a for the field mode, whereas in two-photon decay $R \propto a^2$ [22,23] and in atomic spontaneous emission decay $R \propto \sigma_-$, the Pauli lowering operator for the atomic excitation. Milburn and Wiseman, and others [12,14,36,37] have related these two simulation schemes, the Monte Carlo wave function method, and the quantum-state diffusion method, to specific measurement schemes: the quantum-jump method to continuous direct counting of decay quanta and the quantum-state diffusion method to a heterodyne measurement of oscillation amplitudes. Each has a distinct and characteristic evolution for single realizations. But we should stress that the average over a family of very many realizations generates precisely the ensemble evolution predicted by the density-matrix treatment, quite independent of the particular choice of conditioning. That is, there are many equivalent ways of "unraveling" the master equation, each appropriate to a particular choice of conditioning [12]. The simulation of these individual realizations generates a family of trajectories which, independent of the kind of conditioning used, average to the usual density-matrix predictions of decoherence for the ensemble [4].

In the approach adopted here, the quantum jumps are obtained from conventional quantum mechanics by inclusion of the effects of the larger environment in which the quantum system is embedded. Some authors have examined modifications of the Schrödinger dynamics going beyond conventional quantum mechanics by invoking "intrinsic" mechanisms for decoherence [38]. We have shown elsewhere [39] that for some cases these intrinsic mechanisms act as dephasing rather than dissipative influences in quantum optics. We also wish to stress that we adopt the conventional measurement interpretation of quantum-state diffusion even though quantum-state diffusion has its origins in stochastic quantum mechanics [40].

In Sec. II we first review the treatment of dissipation using the standard master equation form and then we review both the quantum-jump and quantum-state diffusion methods. In Sec. III we explore cases of quantum-state diffusion in more detail and then in Sec. IV we contrast the examples of quantum-state diffusion with the corresponding quantum-jump simulations. Section V concludes this paper.

II. THE MASTER EQUATION AND THE SIMULATION METHODS

A. Density-matrix approach

One standard method for dealing with dissipative problems is the density-matrix approach [41] where the system of interest (a cavity field mode or a single two-level atom, for example) interacts with a reservoir describing the infinite number of degrees of freedom responsible for the irreversible decay. The density matrix describes a lack of precise knowledge about a quantum system. In the current context the lack of knowledge arises from the derivation of the (quantum optics) master equation for the reduced density operator describing the system alone, which involves a trace over the reservoir and results in statistical uncertainty in the state vector.

The system on which we focus in this paper consists simply of a single mode of the radiation field which by virtue of its coupling to some kind of reservoir undergoes dissipation or a loss of energy. As stated in the Introduction, we envisage a mode of the electromagnetic field, but the arguments apply equally to any kind of quantized oscillator. For simplicity, we consider a zero-temperature reservoir, so that the relaxation proceeds purely by spontaneous rather than stimulated transitions. It is straightforward to generalize the argument to include finite-temperature effects [16]. The standard treatment results in the master equation for the density of matrix

$$\frac{d}{dt}\rho=\kappa(\hat{a}\rho\hat{a}^{\dagger}-\tfrac{1}{2}\hat{a}^{\dagger}\hat{a}\rho-\tfrac{1}{2}\rho\hat{a}^{\dagger}\hat{a}) , \tag{1}$$

when the rotating-wave approximation has been made. There is no Hamiltonian term describing the free (nondissipative) evolution because we consider only the decay of a prepared quantum state and because the density matrix ρ is transformed to the interaction representation. However, coherent couplings can be included in a straightforward way. As usual, $\hat{a}$ and $\hat{a}^{\dagger}$ describe the emission and absorption of photons and the symbol κ gives the mean loss rate of energy from the mode.

B. Formalism of quantum-jump simulations

The simulation methods deal with ensembles of pure states where the quantum system of interest decays into a reservoir irreversibly: measurement of the decay products condition the evolution of the state vector describing that particular realization. The simulation proceeds by examining the evolution of single realizations whose state is conditioned by the gain in knowledge acquired through the measurement process. In this way we can dispense with the need to use the density matrix. The evolution of the entire ensemble is then obtained from an appropriate averaging process. Because photon emission events are random and uncontrollable this generally results in a stochastic evolution of the state vector in time. In a computer *simulation* we recreate the history of measurements with the correct likeliness in time. To obtain results that are comparable to those obtained from the master equation (1) we average over an ensemble of state vectors. In the case of such a monitored system the decay rate κ corresponds to the mean absorption rate of photons by the quantum photon counter. For the purposes of the theory we assume a photon counter which is perfectly efficient, but which takes time to absorb the energy of the quantum state that it is measuring. The theory can be extended to detectors with finite efficiency. Simulation methods

such as those we discuss here are motivated by more than a need to describe specific approaches to measurement. The methods can be used as simply a practical way of approximating the solution of a master equation of the type given in Eq. (1), especially when the dimensionality of the system precludes the use of density matrices using modest-size computers.

The quantum jump simulation of histories can be carried out in the following way. We represent the state vector $|\psi(t)\rangle$ as a complex vector within a computer model. Time is discretized in intervals of, say, δt. At any time t the probability for the detection of a photon in a short interval δt is simply given by

$$\Delta P=\kappa\langle\psi(t)|\hat{a}^{\dagger}\hat{a}|\psi(t)\rangle\delta t \ . \tag{2}$$

This is evaluated and compared to a random number to determine whether or not the detection will take place at the given time in the simulation. If a decay quantum is detected, the state vector is modified by a quantum jump; we apply the operator $\hat{a}$ and renormalize

$$|\psi(t)\rangle\rightarrow\frac{\hat{a}|\psi(t)\rangle}{\sqrt{\langle\psi(t)|\hat{a}^{\dagger}\hat{a}|\psi(t)\rangle}} \ . \tag{3}$$

This is sometimes known as a quantum measurement of the second kind [42]. If there is a null result we propagate the state vector over δt with the non-Hermitian Hamiltonian

$$H_{\rm eff}=-\tfrac{1}{2}i\kappa\hat{a}^{\dagger}\hat{a} \ . \tag{4}$$

The state vector must also be renormalized in this case because $H_{\rm eff}$ is non-Hermitian. In this version of the quantum jump method the state vector must be renormalized at every time step to ensure that the transition probabilities (2) are calculated correctly. In a different version of the method [29,31,12,21,32] one calculates a stochastic time interval to the next jump [43] and so less renormalization is required. In general the two steps in the simulation are entirely equivalent to (1) when ensemble averaged as, for example, shown in [12,13,23].

We consider next the form of the state that emerges after m jumps, or detection events, and the probability that m jumps take place during an individual run. We have seen that the general form of the state vector evolution consists of the smooth evolution of Eq. (4) interrupted with the jumps of Eq. (3). Given a sequence of jumps at times $t_1,t_2,t_3,\ldots,t_m$ we analytically calculate the state vector that results. This is found to be a state vector that is conditional on the measurement process: using the rules above one finds that

$$\begin{aligned}|\psi(t)\rangle=&\frac{1}{N_m(t)}e^{-\hat{n}\kappa(t-t_m)/2}\sqrt{\kappa}\hat{a}e^{-\hat{n}\kappa(t_m-t_{m-1})/2}\\&\times\sqrt{\kappa}\hat{a}\cdots e^{-\hat{n}\kappa(t_3-t_2)/2}\\&\times\sqrt{\kappa}\hat{a}e^{-\hat{n}\kappa(t_2-t_1)/2}\sqrt{\kappa}\hat{a}e^{-\hat{n}\kappa t_1/2}|\psi(0)\rangle \ .\end{aligned} \tag{5}$$

(See also Refs. [12,44] for related treatments.) This shows a straightforward sequence of evolution with $H_{\rm eff}$ interspersed with the jumps. The factors $\sqrt{\kappa}$ are included with each of the jumps so that the square of the normalization factor $N_m(t)$ represents the conditional probability of the whole sequence if jumps are only to be found at times t_j. We can renormalize at the end of this sequence because we are supposing now that the times t_m are known; they do not have to be determined from a normalized probability.

This interpretation of $N_m(t)$ and the consistency of $H_{\rm eff}$ and the jump (3) can be illustrated in the following way. We suppose there has been no jump to a time t and we let the symbol $P_{nj}(t)$ stand for the probability of this. So at a later time $t+\delta t$ we may use elementary probability theory to write

$$P_{nj}(t+\delta t)=P_{nj}(t)[1-\Delta P] \ . \tag{6}$$

If we now insert the jump probability from Eq. (3) and take the limit $\delta t\rightarrow 0$ we obtain the differential equation

$$\frac{dP_{nj}(t)}{dt}=-\kappa\langle\psi(t)|\hat{n}|\psi(t)\rangle P_{nj}(t) \ . \tag{7}$$

Now we consider the unnormalized state vector $|\tilde{\phi}(t)\rangle$, which undergoes evolution with $H_{\rm eff}$. (Note that all unnormalized state vectors are denoted with a tilde in this paper). During the period when there is no jump its time evolution is

$$\frac{d}{dt}|\tilde{\phi}(t)\rangle=-iH_{\rm eff}|\tilde{\phi}(t)\rangle=-\frac{\kappa}{2}\hat{n}|\tilde{\phi}(t)\rangle \ , \tag{8}$$

as found in Eq. (5). The relation between $|\psi(t)\rangle$ and $|\tilde{\phi}(t)\rangle$ is simply that

$$|\psi(t)\rangle=\frac{|\tilde{\phi}(t)\rangle}{\sqrt{\langle\tilde{\phi}(t)|\tilde{\phi}(t)\rangle}} \tag{9}$$

and since from Eq. (8) the square of the normalization $\langle\tilde{\phi}(t)|\tilde{\phi}(t)\rangle$ obeys the equation

$$\begin{aligned}\frac{d}{dt}[\langle\tilde{\phi}(t)|\tilde{\phi}(t)\rangle]&=-\kappa\langle\tilde{\phi}(t)|\hat{n}|\tilde{\phi}(t)\rangle\\&=-\kappa\langle\psi(t)|\hat{n}|\psi(t)\rangle\langle\tilde{\phi}(t)|\tilde{\phi}(t)\rangle\end{aligned} \tag{10}$$

we see that it obeys the same equation as $P_{nj}(t)$ and thus, since it has the same initial condition, $P_{nj}(t)$ and $\langle\tilde{\phi}(t)|\tilde{\phi}(t)\rangle$ are identical.

We have now justified Eq. (5) and having identified $[N_m(t)]^2$ with the conditional probability we proceed to simplify the equation by placing the operators $\hat{a}$ together:

$$\begin{aligned}|\psi(t)\rangle&=\frac{(\kappa e^{\kappa t})^{m/2}}{N_m(t)}e^{-\kappa\tau/2}\hat{a}^m e^{-\kappa t\hat{n}/2}|\psi(0)\rangle\\&=\frac{(\kappa)^{m/2}}{N_m(t)}e^{-\kappa\tau/2}e^{-\kappa t\hat{n}/2}\hat{a}^m|\psi(0)\rangle \ ,\end{aligned} \tag{11}$$

where

$$\tau=\sum_{j=1}^{m}t_j \ . \tag{12}$$

Equation (11) shows that all the dependence of the state vector on the jump times t_j is now contained within the parameter τ. This means that the jump times t_j may affect the normalization of the state and hence the probability of the state occurring, but the values t_j do not affect the normalized state: only the number of jumps m is important. This result will prove useful in the construction of normalized states after a given number of jumps.

If we wish to find the probability for a state $|\psi(t)\rangle$ being produced at a time t by any m jumps, we need to integrate the probability $[N_m(t)]^2$ over all the possible t_j that could have produced the state. That is, we require

$$P_m(t)=\int_0^t dt_1 \int_{t_1}^t dt_2 \int_{t_2}^t dt_3 \cdots \int_{t_{m-1}}^t dt_m N_m(t_1,t_2,\ldots,t_m)^2 , \tag{13}$$

where we have included all the time dependence of $N_m(t)$. If we write $[N_m(t)]^2$ as

$$[N_m(t)]^2=(\kappa e^{\kappa t})^m e^{-\kappa\tau}\langle\psi(0)|e^{-\kappa t\hat{n}/2}\hat{a}^{\dagger m}\hat{a}^m e^{-\kappa t\hat{n}/2}|\psi(0)\rangle , \tag{14}$$

we can see from the dependence of τ on the times t_j [Eq. (12)] that Eq. (13) can be rewritten as

$$\begin{aligned} P_m(t)&=\frac{1}{m!}\int_0^t dt_1 \int_0^t dt_2 \int_0^t dt_3 \cdots \int_0^t dt_m N_m(t_1,t_2,\ldots,t_m)^2 \\ &=\frac{(e^{\kappa t}-1)^m}{m!}\langle\psi(0)|e^{-\kappa t\hat{n}/2}\hat{a}^{\dagger m}\hat{a}^m e^{-\kappa t\hat{n}/2}|\psi(0)\rangle . \end{aligned} \tag{15}$$

If the initial photon number distribution is described by the function $P(n)$ the function $P_m(t)$ becomes [42,45]

$$P_m(t)=(e^{\kappa t}-1)^m \sum_{n\geq m} P(n)e^{-n\kappa t}\frac{n!}{m!(n-m)!} . \tag{16}$$

It is satisfying to see that as $t\rightarrow\infty$ the original photon-number distribution is reproduced as $P_m(t)\rightarrow P(m)$.

C. General formalism of quantum-state diffusion

The second kind of simulation method we consider is known as quantum-state diffusion [15]. In this approach there are no distinct jumps of the Wigner function and the state vector continuously diffuses according to the nonlinear stochastic differential equation [15]

$$\begin{aligned} |d\psi\rangle=&\kappa[\langle\hat{a}^\dagger\rangle\hat{a}-\tfrac{1}{2}\hat{a}^\dagger\hat{a}-\tfrac{1}{2}\langle\hat{a}^\dagger\rangle\langle\hat{a}\rangle]|\psi(t)\rangle dt \\ &+\sqrt{\kappa}[\hat{a}-\langle\hat{a}\rangle]|\psi(t)\rangle d\xi_t , \end{aligned} \tag{17}$$

where $d\xi_t$ is a random complex Wiener variable, or Gaussian noise term. It varies randomly between each time step and for each sample run so that when averaged

$$\overline{d\xi_t}=0 , \tag{18}$$

$$\overline{d\xi_t d\xi_{t'}}=0 , \tag{19}$$

$$\overline{d\xi_t^* d\xi_{t'}}=\delta_{t,t'}\delta t . \tag{20}$$

This equation, originally constructed by Gisin and Percival, has recently been interpreted by Wiseman and Milburn as the state vector evolution in a balanced heterodyne detection scheme [36]. A related equation is found for the case of balanced homodyne detection by Carmichael [12]. In both cases a quantum-jump theory is developed for the measurement process in the presence of a strong classical local oscillator. This quantum jump theory, unlike the single mode case presented above, contains two jump operators, i.e., one for each of the detectors. Using the fact that the local oscillator is strong and creates many jumps in the detector, the number of jumps in a short time interval can be determined by a stochastic function $d\xi_t$ as found in Eq. (17) above. Wiseman and Milburn then treat the heterodyne case by smoothing out the fastest oscillations to obtain

$$\begin{aligned} |d\tilde{\psi}\rangle=&\left[-\frac{\kappa}{2}\hat{a}^\dagger\hat{a}dt+\kappa\hat{a}\langle\psi(t)|\hat{a}^\dagger|\psi(t)\rangle dt\right. \\ &\left.+\sqrt{\kappa}\hat{a}d\xi_t\right]|\tilde{\psi}(t)\rangle , \end{aligned} \tag{21}$$

where $|\tilde{\psi}(t)\rangle$ is an unnormalized state vector and $|\psi(t)\rangle$ is the normalized state vector. To obtain the equation of motion for the normalized state vector one has to be careful about differentiation because of the normalization of the noise term [Eq. (20)]. The *Itô* calculus may be used in which, for example,

$$d[\langle\tilde{\psi}(t)|\tilde{\psi}(t)\rangle]=\langle\tilde{\psi}(t)|d\tilde{\psi}\rangle+\langle d\tilde{\psi}|\tilde{\psi}(t)\rangle+\langle d\tilde{\psi}|d\tilde{\psi}\rangle . \tag{22}$$

Furthermore, it is necessary to include a phase factor so that

$$|\psi(t)\rangle=\frac{e^{i\xi(t)}|\tilde{\psi}(t)\rangle}{\sqrt{\langle\tilde{\psi}(t)|\tilde{\psi}(t)\rangle}} . \tag{23}$$

The phase factor is stochastic because

$$id\xi=\frac{\langle\tilde{\psi}(t)|\hat{a}^\dagger|\tilde{\psi}(t)\rangle d\xi_t^*-\langle\tilde{\psi}(t)|\hat{a}|\tilde{\psi}(t)\rangle d\xi_t}{2\langle\tilde{\psi}(t)|\tilde{\psi}(t)\rangle} , \tag{24}$$

resulting in the equation for the normalized $|\psi(t)\rangle$

$$|d\psi\rangle=\kappa[-\tfrac{1}{2}\hat{a}^{\dagger}\hat{a}+\hat{a}\langle\psi(t)|\hat{a}^{\dagger}|\psi(t)\rangle+\tfrac{1}{2}\langle\psi(t)|\hat{a}^{\dagger}\hat{a}|\psi(t)\rangle-\langle\psi(t)|\hat{a}^{\dagger}|\psi(t)\rangle\langle\psi(t)|\hat{a}|\psi(t)\rangle]|\psi(t)\rangle dt$$
$$+\tfrac{1}{2}\kappa[-\langle\psi(t)|\hat{a}^{\dagger}\hat{a}|\psi(t)\rangle+\langle\psi(t)|\hat{a}^{\dagger}|\psi(t)\rangle\langle\psi(t)|\hat{a}|\psi(t)\rangle]|\psi(t)\rangle d\xi_t^* d\xi_t$$
$$+\sqrt{\kappa}[\hat{a}-\langle\psi(t)|\hat{a}|\psi(t)\rangle]|\psi(t)\rangle d\xi_t \ . \tag{25}$$

This equation yields the Gisin-Percival equation (17) given $d\xi_t^* d\xi_t \to dt$ as $dt \to 0$. Our computer program integrates Eq. (17) with a finite step size dt and renormalizes the state vector at every time step.

We should again emphasize that the nonlinear equations we consider here is no way violate the principles of quantum mechanics. Each kind of simulation is nonlinear because it is conditioned on a specific unraveling of the master equation (1) and when we ensemble average over a larger number of state vectors we always recover the master equation (1) [13,12,15,23].

III. QUANTUM-STATE DIFFUSION

A. Localization of a Schrödinger "cat"

As a first example of the localization process in quantum-state diffusion we consider a simple example of a nonclassical state: the Schrödinger "cat." This can be described as a quantum superposition of two macroscopically distinct quantum state. In practice the Schrödinger "cat" states we consider here are at best "mesoscopic," with quite modest quantum numbers, because it makes the calculations more feasible. Cavity QED experiments are likely to be able to investigate such mesoscopic "cats" [9,10]. The trend for truly macroscopic Schrödinger "cats" is fairly clear. The particular type of Schrödinger "cat" we focus on consists of a superposition of two coherent states $|\alpha\rangle$ and $|-\alpha\rangle$ in the form

$$|\alpha,\pm\rangle=\frac{|\alpha\rangle\pm|-\alpha\rangle}{N_{\pm}(\alpha)} \ , \tag{26}$$

where $N_{\pm}(\alpha)$ is the normalization

$$N_{+}(\alpha)=2e^{-|\alpha|^2/2}\sqrt{\cosh|\alpha|^2} \ ,$$
$$N_{-}(\alpha)=2e^{-|\alpha|^2/2}\sqrt{\sinh|\alpha|^2} \ . \tag{27}$$

We restrict ourselves here to these two types of Schrödinger "cat" with the two signs. The state $|\alpha,+\rangle$ is known as the even coherent state because it only has even numbers in its photon-number distribution and likewise the state $|\alpha,-\rangle$ is known as the odd coherent state [46,47].

Using the even and odd coherent states as initial states we have computed the time evolution of the state vector following the quantum-state diffusion of Eq. (17). The most striking feature of this evolution is localization [15,19,23]; very rapidly one of the two components of the Schrödinger "cat" is selected. This is very visibly demonstrated by using a phase-space representation of the state. We use the Wigner quasiprobability function because of the way it demonstrates the existence of quantum interference through the presence of phase-space interference. The Wigner function also yields the correct marginal distributions when integrated and can be inferred experimentally from such measurable marginals [48]. We calculate the Wigner function from the state vector using the method outlined in Ref. [49]; if the state vector is expressed in the Fock basis as

$$|\psi(t)\rangle=\sum_{n=0}^{\infty} a_n(t)|n\rangle \ , \tag{28}$$

then the Wigner function is found in polar coordinates as

$$W(r,\theta)=\sum_{m,n} a_m a_n^* W_{mn}(r,\theta) \ , \tag{29}$$

where

$$W_{mn}(r,\theta)=\frac{2}{\pi}(-1)^n\left[\frac{n!}{m!}\right]^{1/2} e^{i(m-n)\theta}$$
$$\times(2r)^{m-n}e^{-2r^2}L_n^{m-n}(4r^2) \tag{30}$$

for $m \geq n$. The results are subsequently given in the Cartesian coordinate system: $X=r\cos\theta$, $Y=r\sin\theta$.

Figure 1 shows a typical example of the localization process. The initial Wigner function for an even coherent state is seen in Fig. 1(a) with its dominating fringes between the components of the Schrödinger "cat." In Fig. 1(b) the Wigner function shows that the state is clearly approaching one of the components and within a very short time [Fig. 1(c)] the fringes have nearly completely disappeared. In Fig. 1(d) we much more closely approach one of the coherent-state components. Subsequently this coherent state subsides to the vacuum state during the final stages of the dissipative process.

We reported in Ref. [24] that the uncertainty

$$\Delta X=\sqrt{\langle\hat{X}^2\rangle-\langle\hat{X}\rangle^2} \ , \tag{31}$$

where $\langle\hat{X}\rangle=\langle\psi(t)|(\hat{a}+\hat{a}^{\dagger})|\psi(t)\rangle/2$, shows the localization process by a very rapid reduction to the coherent state value of one-half; see the dotted curve in Fig. 2(a). The same is true of ΔY [though it is not seen in Fig. 2(b)]. During the localization period a nonzero value of $\langle\hat{X}\rangle$ is formed which thereafter slowly decays as the selected coherent-state component relaxes to the vacuum; this can be seen in the solid curve of Fig. 3. A remarkable feature of these simple Schrödinger "cats" is that, although $\langle\hat{X}\rangle, \Delta X$, and ΔY behave in a partly random way, the expectation value of the number operator $\langle\hat{n}\rangle$ does not. It decays smoothly to zero exactly as for the density matrix case (see Fig. 4).

The time scale of the localization is faster if the Schrödinger "cat" components are larger. In fact the loss of the fringes by localization seems to take place at the same rate as the loss of fringes in the density matrix

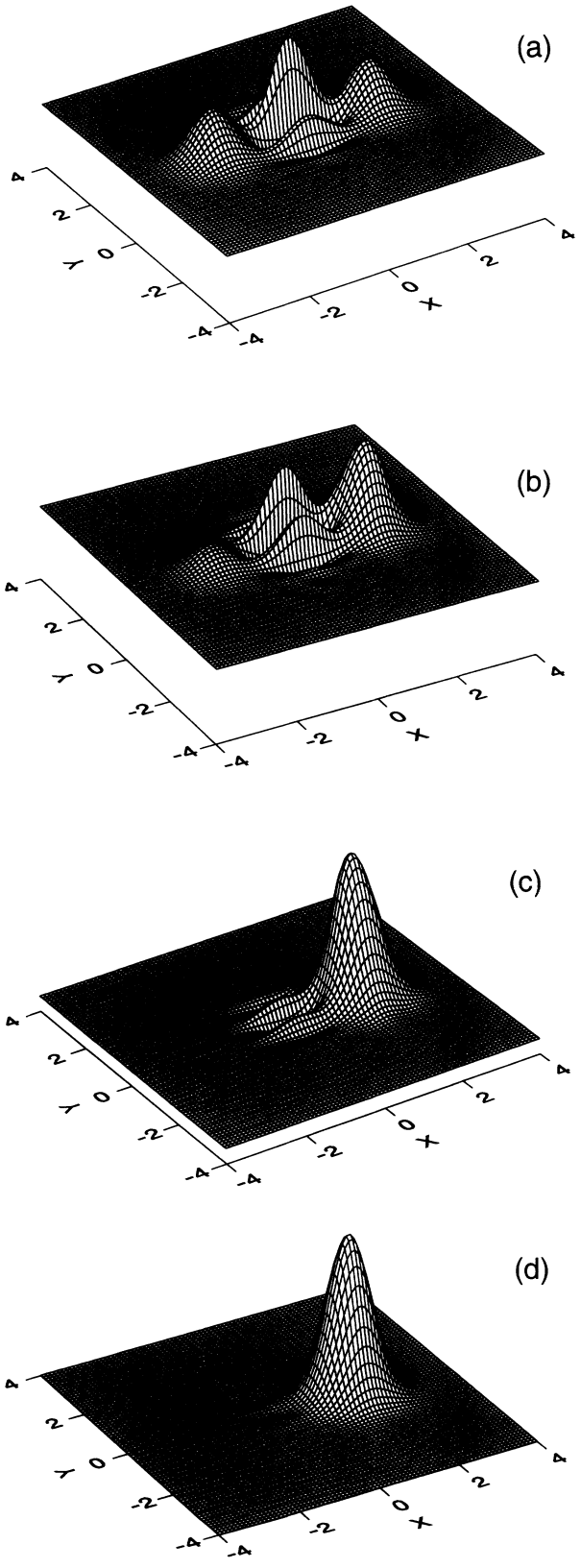


FIG. 1. Localization of a Schrödinger "cat" state which is initially the even coherent state $|2.0,+\rangle$ as defined in Eq. (26). These results are an example of a single sample undergoing quantum-state diffusion. We depict the Wigner functions for $\kappa t = 0$, 0.1, 0.2, and 0.5 in (a)–(d). Localization is seen as the increasing dominance of one component of the "cat."

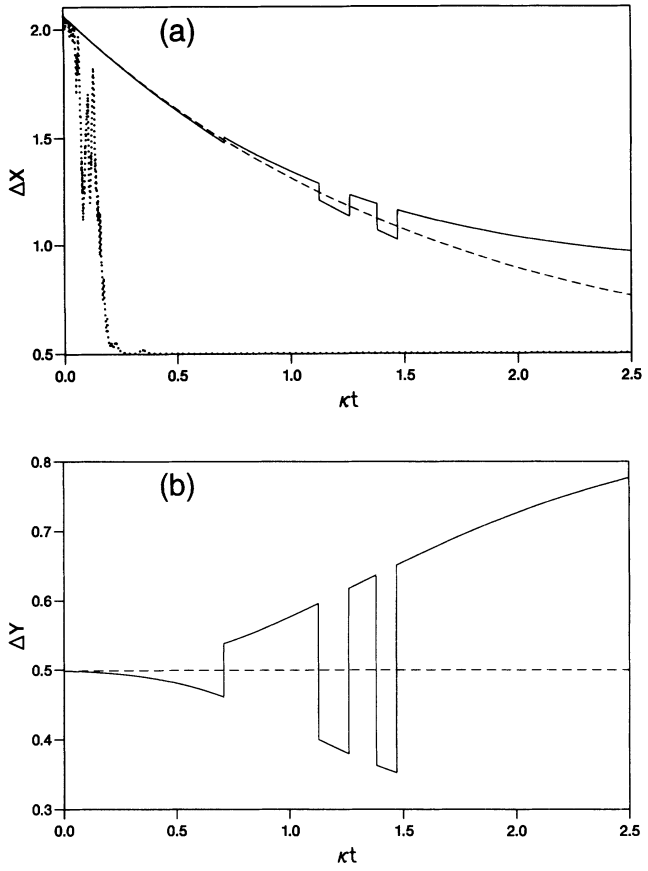


FIG. 2. A plot of the fluctuations (a) ΔX and (b) ΔY. The parameters are the same as in Fig. 1. In both (a) and (b) the solid curve shows the quantum-jump simulation and the dashed curve shows the density matrix result. The dotted curve in (a) is the result of the quantum-state diffusion calculation. In (b) the quantum-state diffusion and density-matrix results cannot be distinguished.

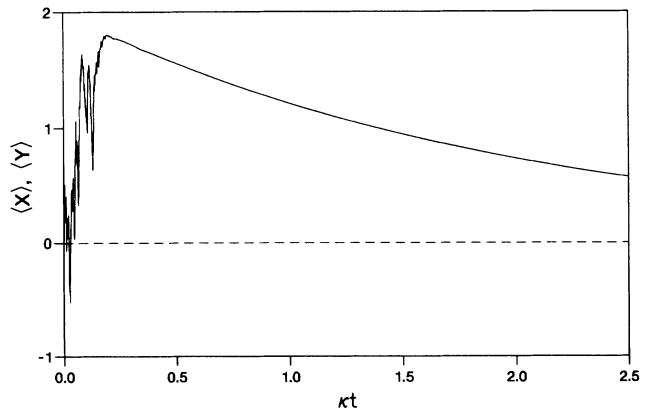


FIG. 3. A plot of the mean value of the quadrature $\langle \hat{X} \rangle$ for quantum-state diffusion (solid curve) and the parameters of Figs. 1 and 2. The density matrix and quantum-jump result for $\langle \hat{X} \rangle$ (dashed curve) are always zero. All three methods give a zero result for $\langle \hat{Y} \rangle$ because of the symmetry of the problem.

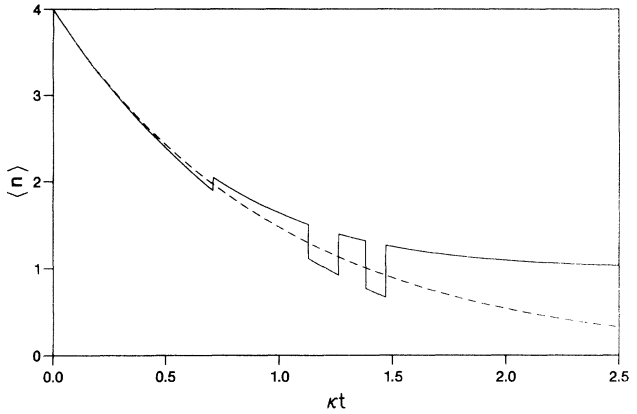


FIG. 4. The mean photon number for an initial Schrödinger "cat" and the same parameters as in Fig. 1. The solid curve shows the quantum-jump simulation as the Schrödinger "cat" evolves and jumps towards the vacuum. The dashed curve indicates the result from the density-matrix treatment *and* the quantum-state diffusion simulation. In the latter case the curve also relates to Fig. 1.

treatment. Of course, in the density matrix case there is no localization; once the Wigner fringes have gone an equal mixture of two components is left [50].

B. Localization of a Fock state

The Fock state, an eigenstate of the harmonic oscillator, is a very nonclassical state and does not remain intact for very long under the influence of dissipation [2]. In a quantum-state diffusion simulation or heterodyne measurement, the state localizes and approaches a coherent state. The process is illustrated in Fig. 5 for the initial state $|n\rangle$ with $n=9$. The initial Wigner function, as described by W_{nn} in Eq. (30), is shown in Fig. 5(a). During a short space of time [Figs. 5(b) and 5(c)], the Wigner function loses its circular structure and eventually collapses into a single peak located close to the outer rim of the initial Wigner function [Fig. 5(d)]. During this process the mean photon number $\langle \hat{n} \rangle$ simply decays in a roughly exponential, though stochastic, manner as can be seen in Fig. 6. A decay can also be seen in the mean values of the quadratures $\langle \hat{X} \rangle$ and $\langle \hat{Y} \rangle$ in Fig. 7, but only after nonzero values of these quantities have been established. The initial state had zero values of $\langle \hat{X} \rangle$ and $\langle \hat{Y} \rangle$ and the development of definite nonzero values is another manifestation of the localization process. As in the case of the Schrödinger "cat," localization can be seen in the fluctuations ΔX and ΔY in Fig. 8. These fluctuations reduce to one-half, which is the value for a coherent state. However, the rate of the reduction is rather less rapid when compared to the even coherent state of Fig. 3.

We may suppose that in the localization process the initial state may be regarded as divided into coherent states from which one component is selected. In the case of the Schrödinger "cat" we had a choice of two components. In the case of a Fock state there are an infinite number of components because we can write the Fock state as [51]

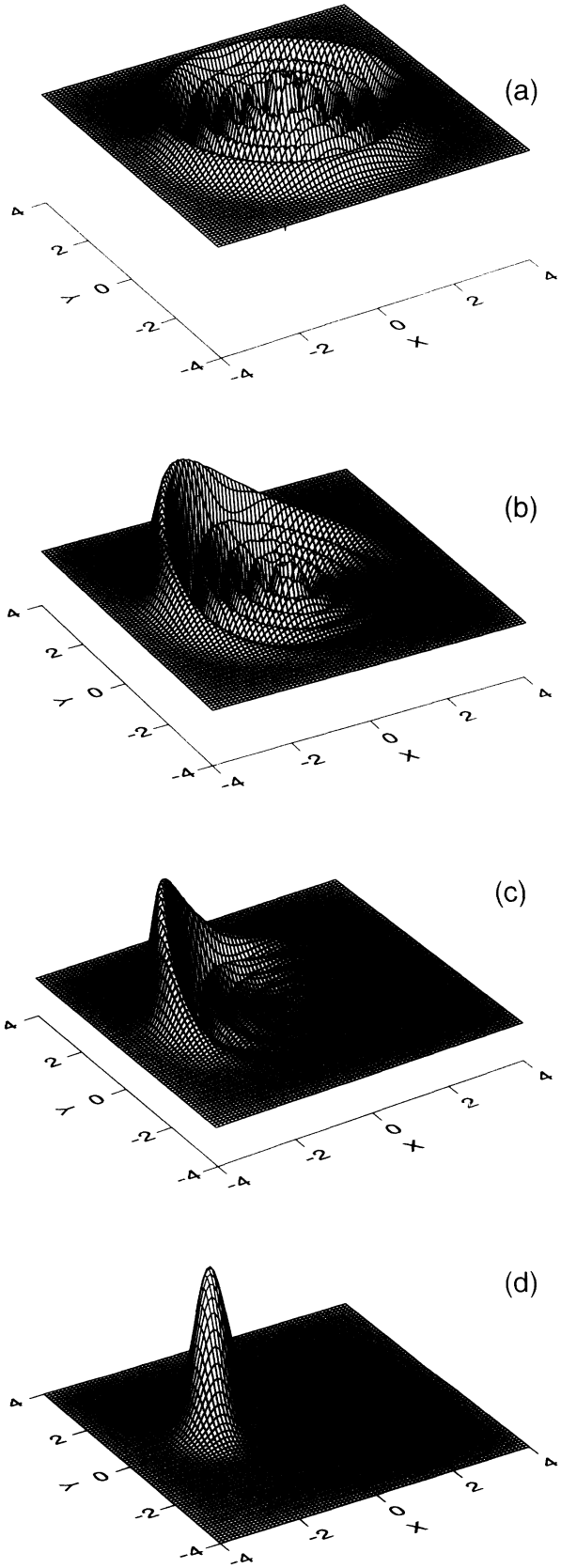


FIG. 5. Localization of a Fock state with $n=9$. These results are for a single sample undergoing quantum-state diffusion. The Wigner functions are shown for $\kappa t=0$, 0.1 0.2, and 1.0 in (a)–(d).

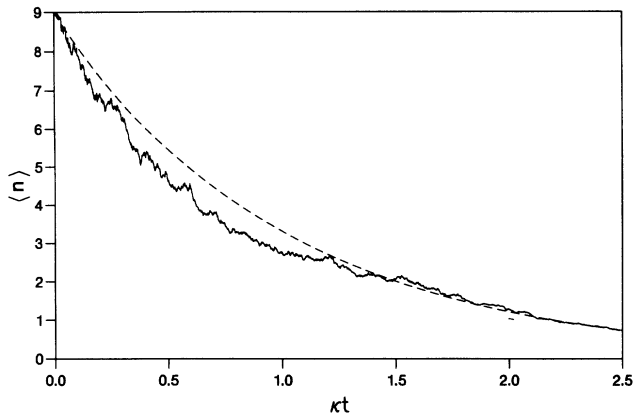


FIG. 6. The mean photon number from quantum-state diffusion (solid curve) and a density-matrix treatment (dashed curve). The initial state was the Fock state $|9\rangle$ and the Wigner functions are presented in Fig. 5.

$$|n\rangle = \frac{e^{r^2/2}\sqrt{n!}}{2\pi r^n}\int_0^{2\pi} d\theta\, e^{-in\theta}|re^{i\theta}\rangle \ . \tag{32}$$

This shows the Fock state to be a superposition of coherent states $|re^{i\theta}\rangle$ around a ring of radius r. Any of these states could be selected when localization takes place provided the radius of the ring of coherent states is such that the coherent state that is selected has the correct energy.

This picture of localization is, however, only approximate. If we examine Eq. (17) or (25) we will observe that the change in the state vector is always such as to produce a superposition of Fock states including and below the initial Fock state. This is because the only operators that act on $|\psi(t)\rangle$ are $\hat{a}$ or $\hat{a}^\dagger\hat{a}$; there are no operators that will connect the state to higher Fock states. After localization takes place the photon-number distribution resembles that of a coherent state, but it is bounded within an upper limit, as may be seen in Fig. 9. Thus it is

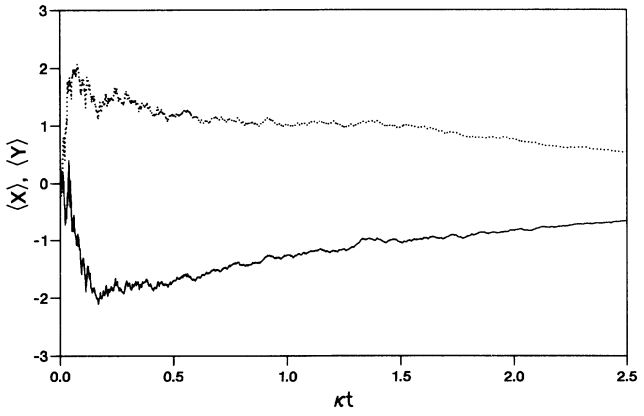


FIG. 7. Mean values of the quadratures for the example of quantum-state diffusion presented in Fig. 6. The mean values are zero in a quantum jump or density-matrix treatment and become nonzero in the case of quantum-state diffusion because of the localization process. The solid curve is $\langle \hat{X} \rangle$ and the dotted curve is $\langle \hat{Y} \rangle$.

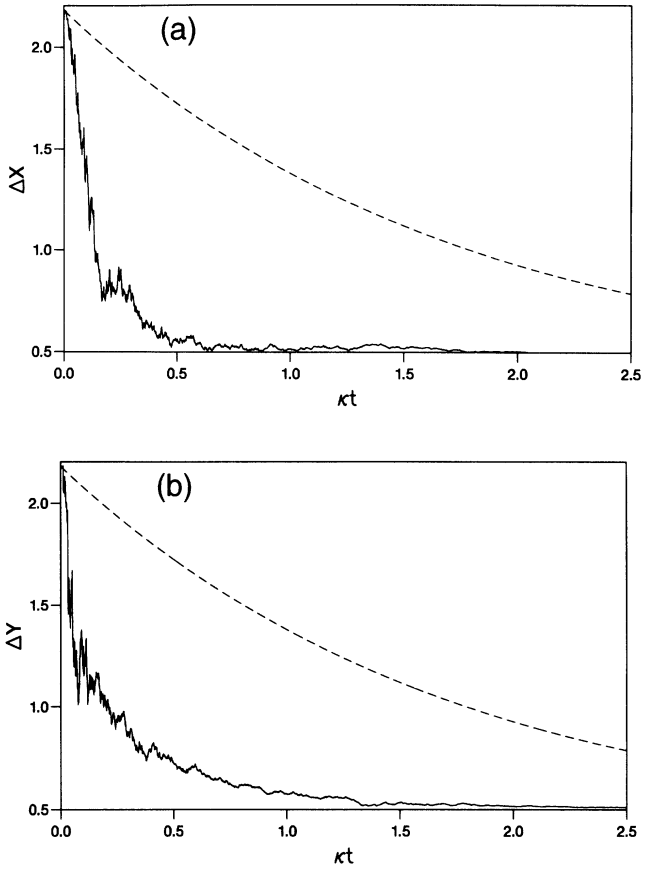


FIG. 8. The fluctuations in the quadratures (a) ΔX and (b) ΔY for the example of quantum-state diffusion presented in Fig. 6. The solid curve shows the quantum-state diffusion result and the dashed curve shows the result from a density-matrix computation.

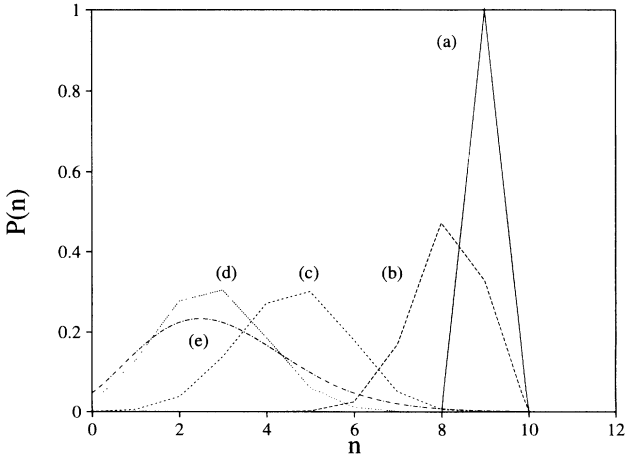


FIG. 9. Photon-number distributions for the localizing Fock state portrayed in Fig. 5. We show $\kappa t = 0.0$, 0.1, 0.5, and 1.0 by the curves (a)–(d). The photon-number distribution for a coherent state with a mean energy of three photons is shown by (e).

necessary for the peak in the photon-number distribution at n to lie at least $\sqrt{n}$ away from the initial photon number of the Fock state (n_0 say) for localization to be completed. A simple calculation shows that for large n_0 we achieve this condition if $n \sim n_0 - \sqrt{n_0}$. Now n gives the mean energy at the localization time t_l and n_0 gives the initial energy. Because the decay of the mean photon number is roughly exponential (see, for example, Fig. 6) it follows that $n \sim n_0 \exp(-\kappa t_l)$, which yields the estimate for the localization time $\kappa t_l \sim 1/\sqrt{n_0}$. Clearly, the time taken for localizing decreases as the initial photon number increases.

C. Localization of the squeezed vacuum

The squeezed vacuum may be defined from the action of the squeeze operator on the vacuum state [52],

$$|s,\theta\rangle = \exp\{(s/2)[(\hat{a}^\dagger)^2 e^{i\theta} - \hat{a}^2 e^{-i\theta}]\}|0\rangle \ , \qquad (33)$$

where s is the squeezing factor. Unlike the Fock state, the squeezed vacuum has an orientation in phase space, a feature it shares with the Schrödinger "cat." This axis of orientation is at an angle of $\theta/2$ to the phase-space axes and the Wigner function of the state is a squeezed Gaussian function as shown in Fig. 10(a) for $s=0.8$. Because the squeezed vacuum has this orientation we may suppose that the localization process will be more definite

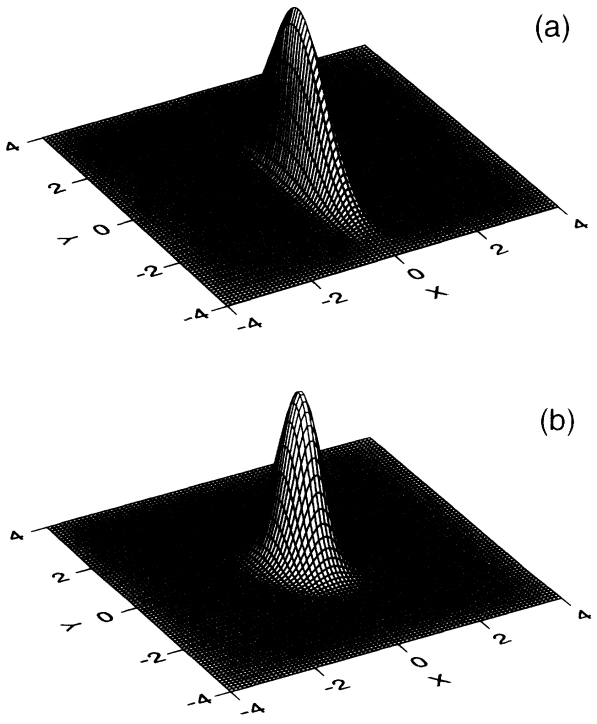


FIG. 10. Wigner functions in a quantum-state diffusion simulation starting from a squeezed vacuum state [Eq. (33)] with $s(0)=0.8$ and $\theta=0$. In (a) we show the initial state and in (b) we show the Wigner function when $\kappa t=1.0$. In the latter case the Wigner function has lost much of its squeezing, but is displaced from the phase-space origin.

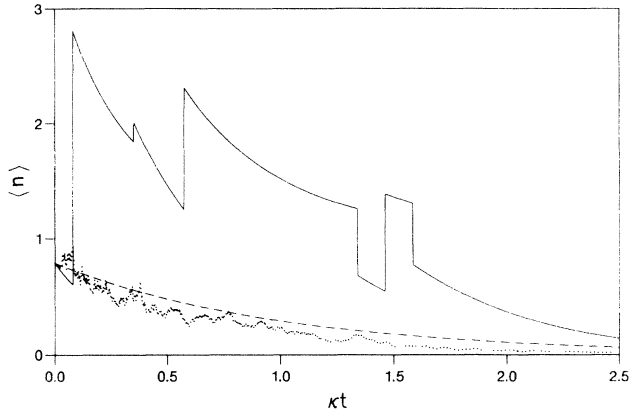


FIG. 11. Mean photon number from an initial squeezed vacuum [Eq. (33)] with $s(0)=0.8$ as in Fig. 10. The solid curve shows the quantum-jump simulation, the dotted curve shows the quantum-state diffusion simulation, and the dashed curve shows the result from the density-matrix calculation.

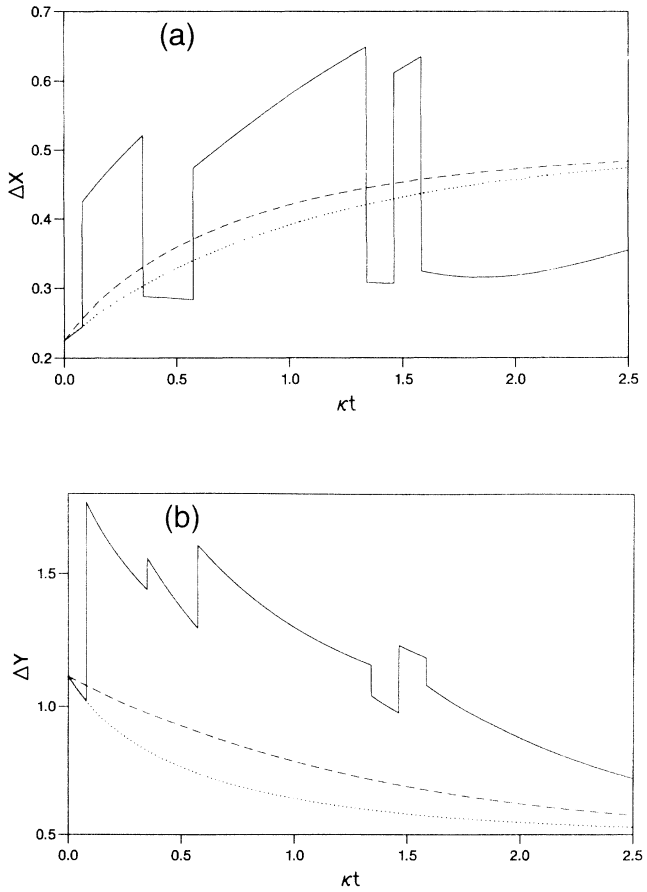


FIG. 12. Fluctuations in the quadratures during evolution from an initial squeezed vacuum. The parameter and curves are defined in Fig. 11. Note that under quantum-state diffusion ΔX and ΔY are smooth curves, unlike the quantum-state diffusion result for $\langle \hat{n} \rangle$ seen in Fig. 11.

than in the case of a Fock state. This is because of the connection to a heterodyne measurement, an amplitude measure, which was outlined in Sec. II C. Indeed, in Fig. 10(b) we can see evidence of localization in the displacement of the Wigner function from the phase-space origin. As in the case of the Fock states the localization can be regarded as state selection from a group of coherent states. The squeezed vacuum can be expressed in terms of Gaussian distribution of coherent states along a line in phase space such that [51]

$$|s,\theta\rangle=(2\pi\sinh s)^{-1/2}\times\int_{-\infty}^{\infty}dr\,\exp[-r^2/(e^{2s}-1)]|re^{i\theta/2}\rangle\ . \quad (34)$$

This means that localization is more likely near the center of the distribution.

In Fig. 11 the dotted line shows the decay of the mean photon number during the decay process. As expected it is stochastic, but loosely follows the density-matrix result which is shown as the dashed line. The surprising result is found in Fig. 12, where we see that the fluctuations ΔX and ΔY follow smooth curves. (Compare this to the quantum-state diffusion simulation of $\langle\hat{n}\rangle$ in Fig. 4.) In both cases the fluctuations steadily approach the coherent state value of one-half. This localization is less rapid than in the case of the Schrödinger "cat." Note that to obtain the master-equation result for ΔX from the simulations it is necessary to ensemble average over $\langle\hat{X}\rangle$ and $\langle\hat{X}^2\rangle$ separately and then compute ΔX from these averages.

IV. QUANTUM JUMPS AND THE DECAY OF NONCLASSICAL STATES

A. The "jumping cat"

In this section we will consider the quantum jump theory of an initial Schrödinger "cat" such as the even and odd coherent states of Sec. III A. The results will be contrasted with quantum-state diffusion. The quantum jump theory naturally divides into two parts: the non-Hermitian evolution and the jumps themselves. We consider the non-Hermitian evolution first.

To determine the non-Hermitian evolution with $H_{\rm eff}$ [Eq. (4)] we simply have to expand the coherent states in the Fock basis to find that

$$|\psi_0(t)\rangle=\frac{e^{\kappa t\hat{a}^\dagger\hat{a}/2}}{N_0(t)}|\alpha,\pm\rangle=|\alpha e^{-\kappa/2},\pm\rangle\ , \quad (35)$$

where the normalization factor was

$$N_0(t)^2=\begin{cases}\dfrac{\cosh(|\alpha^2|e^{-\kappa t})}{\cosh|\alpha|^2} & \text{(even coherent state)}\\ \dfrac{\sinh(|\alpha^2|e^{-\kappa t})}{\sinh|\alpha|^2} & \text{(odd coherent state)}\ .\end{cases} \quad (36)$$

The normalized state (35) represents a Schrödinger "cat" that shrinks in time (see Fig. 3); both of the components of the "cat" move towards the phase-space origin while

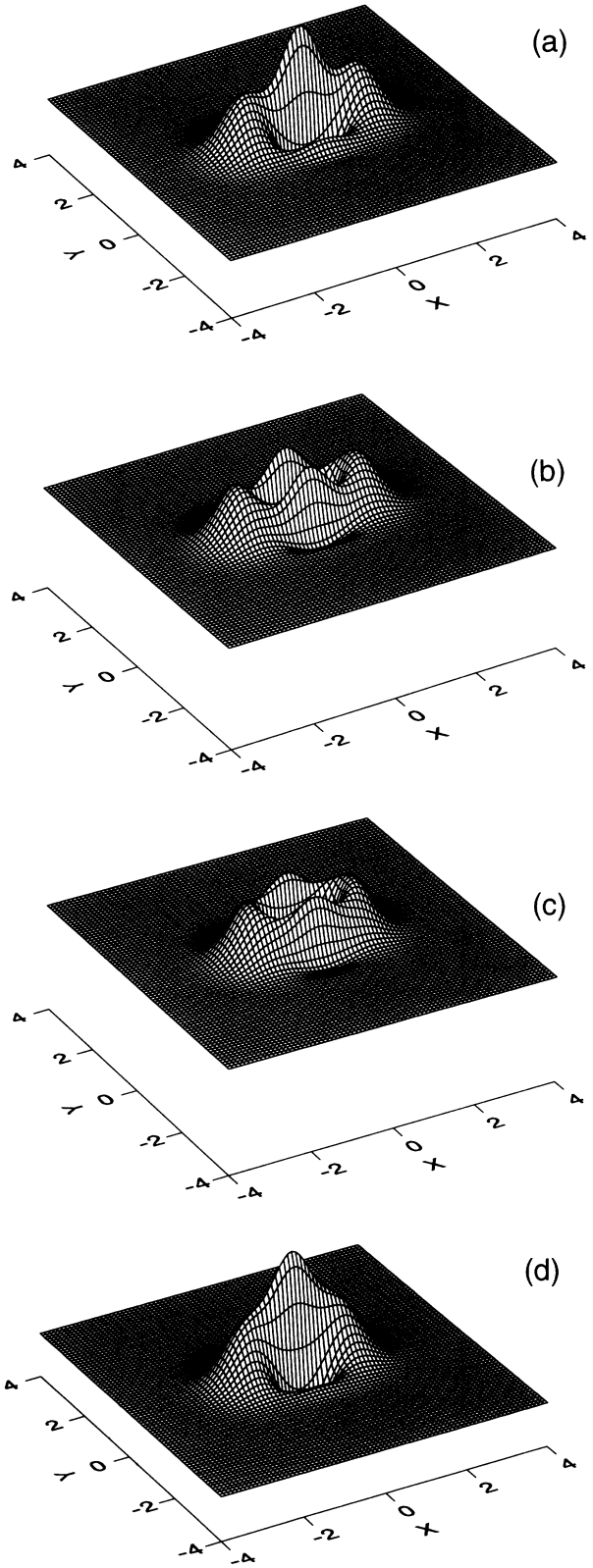


FIG. 13. A "jumping cat" that was initially comprised of the coherent states $|\alpha\rangle$ and $|-\alpha\rangle$ with $\alpha=2$. These results are for a single sample where the internal phase of the cat changes at each quantum jump. We show the Wigner functions before and after the first jump (at $\kappa t=0.708$) in (a) and (b). In (c) and (d) we show the Wigner functions before and after the second jump (at $\kappa t=1.127$). The same jumps are seen in Figs. 2–4.

the coherence of superposition is maintained because it is a pure state. The time-dependent probability (36) indicates, as expected, that as $t \to \infty$ it is impossible for the odd coherent state to avoid at least one jump while there is a finite probability of $1/\cosh|\alpha|^2$ that the even coherent state never performs a quantum jump at all.

At any time during this shrinking process the probability (per unit time) of a quantum jump is given by Eq. (2) as

$$\kappa\langle\psi(t)|\hat{n}|\psi(t)\rangle = \begin{cases} \tanh|\alpha(t)|^2 & \text{(even coherent state)} \\ \coth|\alpha(t)|^2 & \text{(odd coherent state)} , \end{cases} \tag{37}$$

where for the shrinking "cat"

$$\alpha(t) = e^{-\kappa t}\alpha(0) . \tag{38}$$

When the Schrödinger "cat" jumps the state vector transforms as [Eq. (3)]

$$|\alpha, \pm\rangle \to |\alpha, \mp\rangle , \tag{39}$$

which means that the Schrödinger "cat" jumps from one type of "cat" to another type of "cat." (See Fig. 13.) During the complete evolution of jumps and non-Hermitian evolution we find that there are essentially only two quantum trajectories: the shrinking even coherent state and the shrinking odd coherent state. The effect of the quantum jumps is simply to switch from one of these trajectories to the other, or vice versa. This is seen clearly in Fig. 4, which shows by the solid curve the mean photon number of the Schrödinger "cat" state as its evolves and jumps. Similar behavior is seen in Fig. 2 for the fluctuation ΔX and especially in ΔY because the even coherent state shows slight squeezing in ΔY whereas the odd coherent state does not.

The principal conclusion in this section is that under continuous photodetection a Schrödinger "cat" remains a Schrödinger "cat" as it relaxes to the vacuum state. Thus the coherence of the two components is maintained by watching the "cat." Unlike the quantum Zeno effect this kind of watching does not prevent the decay, it prevents the decay of the coherence. If we were to consider a different type of superposition we may find a different result. For example, if we have a superposition of a coherent state $|\beta\rangle$ and the vacuum we would have a type of Schrödinger "cat" considered in Ref. [10]. However, as soon as there has been a single quantum jump we would only have the single component $|\beta(t)\rangle$ left [where $\beta(t) = \exp(-\kappa t)\beta(0)$]. This reflects the gain of information when a photon leaves the system; as soon as we detect a photon the possibility of the state $|0\rangle$ is excluded.

B. Quantum jumps and Fock states

We consider the case of quantum jumps and Fock states here only for completeness because their case is very straightforward. The non-Hermitian evolution (4) has no effect on the state after renormalization, as the jumps (3) cause downwards transitions from Fock state to Fock state. The state vector remains nonclassical throughout the evolution. For a Fock state $|n\rangle$ the probability of m jumps up to a time t is given by Eq. (16):

$$P_m(t) = (e^{\kappa t} - 1)^m e^{-n\kappa t} \frac{n!}{m!(n-m)!} . \tag{40}$$

C. Quantum jumps and the squeezed vacuum

An account of a related problem has been given by Ogawa, Ueda, and Imoto in Ref. [53] where they examined the Husimi function of the density matrix after one and two photocounts. The initial state in that case was a displaced squeezed vacuum. Here we will present an analysis in terms of the pure state evolution that will be valid for any number of quantum jumps or photocounts. We consider the squeezed vacuum without any displacement. We will give details of the integral representation of the time-dependent state in terms of coherent states and its relation to a Schrödinger "cat" as the number of jumps increases. However, we first consider the evolution of the state under the effective Hamiltonian H_{eff} and then we look at the effect of the quantum jumps.

The evolution of $|\psi(t)\rangle$ under only the non-Hermitian H_{eff} results in the state vector

$$|\psi_0(t)\rangle = \frac{1}{N_0(t)} e^{-\kappa t\hat{a}^\dagger\hat{a}/2}\hat{S}(s,\theta)|0\rangle , \tag{41}$$

where

$$\hat{S}(s,\theta) = \exp\left\{\frac{s}{2}[(\hat{a}^\dagger)^2 e^{i\theta} - \hat{a}^2 e^{-i\theta}]\right\} \tag{42}$$

as in Eq. (33). As before, the normalization $N_0(T)$ is required because H_{eff} is non-Hermitian and the state vector would otherwise shrink. To proceed we note that

$$\begin{aligned} |\psi_0(t)\rangle &= \frac{1}{N_0(t)} e^{-\kappa t\hat{a}^\dagger\hat{a}/2}\hat{S}(s,\theta)e^{\kappa t\hat{a}^\dagger\hat{a}/2}e^{-\kappa t\hat{a}^\dagger\hat{a}/2}|0\rangle \\ &= \frac{1}{N_0(t)} \exp\left[\frac{s}{2}[(\hat{a}^\dagger)^2 e^{i\theta}e^{-\kappa t} \right. \\ &\qquad \left. - \hat{a}^2 e^{-i\theta}e^{\kappa t}]\right]|0\rangle . \end{aligned} \tag{43}$$

We can rephrase this result by first disentangling the operators using the SU(1,1) disentangling expressions [54] and then reentangling the result as a new squeezed state. The disentangling results in the state

$$\begin{aligned} |\psi_0(t)\rangle &= \frac{1}{N_0(t)\sqrt{\cosh s}} \\ &\quad \times \exp[e^{i\theta-\kappa t}\tanh s(\hat{a}^\dagger)^2/2]|0\rangle , \end{aligned} \tag{44}$$

and when we reentangle we obtain the state as

$$|\psi_0(t)\rangle = \hat{S}[s(t),\theta]|0\rangle , \tag{45}$$

where the normalization was found as

$$N_0(t) = \left[\frac{\cosh s(t)}{\cosh s(0)}\right]^{1/2} . \tag{46}$$

The time-dependent squeezing factor is found to be given from

$$\tanh s(t)=e^{-\kappa t}\tanh s(0)\ . \tag{47}$$

Thus we see that the effect of the non-Hermitian evolution is to decrease the squeezing of the state. The probability of continuous evolution without a quantum jump is given by $N_0(t)^2$.

To obtain the quantum state after m jumps we recall Eq. (11) and using Eqs. (41)–(47) the normalized state vector is found as

$$|\psi_m(t)\rangle=\frac{(\kappa e^{\kappa(t-\tau)})^{m/2}}{N_m(t)}\hat{a}^m\hat{S}[s(t),\theta]|0\rangle\ . \tag{48}$$

To find the probability of reaching this state we would require the normalization factor $N_m(t)$, although we will focus on the state itself rather than the probability of finding it, and so write it in the form

$$|\psi_m(t)\rangle=\frac{1}{N'_m(t)}\hat{a}^m\hat{S}[s(t),\theta]|0\rangle\ . \tag{49}$$

The photon-number distribution and Fock state expansion are found from the Fock state expansion of the squeezed vacuum [55]:

$$\begin{aligned}\frac{\hat{a}^m}{N'_m(t)}\hat{S}[s(t),\theta]|0\rangle&=\frac{\hat{a}^m}{N'_m(t)\sqrt{\cosh s(t)}}\sum_{l=0}^{\infty}\left[\frac{\tanh s(t)e^{i\theta}}{2}\right]^l\frac{\sqrt{(2l)!}}{l!}|2l\rangle\\&=\frac{1}{N'_m(t)\sqrt{\cosh s(t)}}\sum_{m+n\ \text{even}}\left[\frac{\tanh s(t)e^{i\theta}}{2}\right]^{(m+n)/2}\frac{(m+n)!}{[(m+n)/2]!\sqrt{n!}}|n\rangle\ .\end{aligned} \tag{50}$$

The photon-number distribution contains only even photon numbers or only odd photon numbers depending on the number of jumps. We can now formally derive the normalization $N'_m(t)$ from

$$\begin{aligned}[N'_m(t)]^2=&\frac{1}{\cosh s(t)}\\&\times\sum_{m+n\ \text{even}}\left[\frac{\tanh s(t)e^{i\theta}}{2}\right]^{m+n}\\&\times\frac{[(m+n)!]^2}{\{[(m+n)/2]!\}^2 n!}\ .\end{aligned} \tag{51}$$

This is an infinite sum; later we will find a better expression in the form of a finite sum.

To obtain the integral representation of the new state (49) in terms of coherent states we may extend Eq. (34) so that [56]

$$\begin{aligned}|\psi_m(t)\rangle=&\frac{e^{im\theta/2}}{N'_m(t)\sqrt{2\pi\sinh s(t)}}\\&\times\int_{-\infty}^{\infty}dr\exp[-r^2/(e^{2s(t)}-1)]\\&\times r^m|re^{i\theta/2}\rangle\ ,\end{aligned} \tag{52}$$

as can be verified from the Fock state expansion. Thus the distribution of coherent states is the Gaussian of the squeezed vacuum modified by r^m. The integral representation (52) leads to a better expression for the normalization. We obtain first

$$\begin{aligned}\langle n|\psi(t)\rangle=&\frac{e^{i(m+n)\theta}}{N'_m(t)\sqrt{2\pi\sinh s(t)n!}}\\&\times\int_{-\infty}^{\infty}dr\exp[-r^2/(2\tanh s(t))]r^{m+n}\ ,\end{aligned} \tag{53}$$

so that

$$\begin{aligned}P(n)=&\frac{1}{2\pi\sinh s(t)[N'_m(t)]^2 n!}\\&\times\int\int dx\,dy\exp\{-(x^2+y^2)/[2\tanh s(t)]\}\\&\times(xy)^{m+n}\end{aligned} \tag{54}$$

and thus

$$\begin{aligned}[N'_m(t)]^2=&\frac{1}{2\pi\sinh s(t)}\\&\times\int\int dx\,dy\exp\{-(x^2+y^2)/[2\tanh s(t)]\\&+xy\}(xy)^m\ ,\end{aligned} \tag{55}$$

which can be expressed in polar coordinates. When the radial integral is carried out we obtain

$$[N'_m(t)]^2=\frac{m!}{2}\int_0^{2\pi}d\theta\frac{(\sin\theta\cos\theta)^m}{[\frac{1}{2}\coth s(t)-\sin\theta\cos\theta]^{m+1}}\ , \tag{56}$$

which can be integrated to give the finite series

$$\begin{aligned}[N'_m(t)]^2=&2\pi\sinh s(t)m!\left[\frac{\tanh s(t)}{2[1-\tanh s(t)]}\right]^m\\&\times\sum_{l=0}^{m}\left[\frac{\tanh s(t)-1}{\tanh s(t)+1}\right]^l\\&\times\frac{(2m-2l-1)!!(2l-1)!!}{(m-l)!l!}\ .\end{aligned} \tag{57}$$

This series is easier to calculate than the infinite series (51) above. The first few values yields

$$N_0'=1\ ,$$
$$N_1'=\sinh s(t)\ ,$$
$$N_2'=\sqrt{3}\sinh^2 s(t)\ , \tag{58}$$
$$N_3'=\sqrt{3}\sinh^6 s(t)\sqrt{2+3\coth^2 s(t)}\ .$$

We can also use the integral representation (52) to examine the state (49) for large m. By carrying out a saddle-point approximation on the function in the integrand we obtain

$$|\psi_m(t)\rangle \sim \frac{e^{im\theta/2}}{N_m'(t)\sqrt{2\pi\sinh s(t)}} e^{-m/2} \sum_{\pm} (\pm r_0)^m \int_{-\infty}^{\infty} dr \exp[-2(r\pm r_0)^2/(e^{2s(t)}-1)]|re^{i\theta/2}\rangle\ , \tag{59}$$

where

$$r_0(t)=\sqrt{m\{\exp[2s(t)]-1\}/2}=\left[\frac{m\tanh s(0)}{e^{-\kappa t}-\tanh s(0)}\right]^{1/2}. \tag{60}$$

Now a more general squeezed state, the squeezed and displaced vacuum

$$|s,\theta,\alpha\rangle=\hat{D}(\alpha)\hat{S}(s,\theta)|0\rangle\ , \tag{61}$$

(where $\hat{D}$ represents the displacement operator) has the representation in terms of coherent states

$$|s,\theta,\alpha\rangle=(2\pi\sinh s)^{-1/2} \times\int_{-\infty}^{\infty} dr \exp[-r^2/(e^{2s}-1) +ir\,\mathrm{Im}(\alpha e^{-i\theta/2})]|\alpha+re^{i\theta/2}\rangle\ . \tag{62}$$

By comparing the approximate representation of the state for large m with Eq. (62) for the squeezed state we can see that Eq. (59) approximates a superposition of two squeezed states located at $\pm r_0 e^{i\theta/2}$ in phase space. Thus the state (49) may be approximated as

$$|\psi_m(t)\rangle \sim \frac{1}{N_m''(t)}[|s',\theta,r_0\rangle+(-1)^m|s',\theta,-r_0\rangle] \tag{63}$$

with $N_m''(t)$ found from the overlap of the squeezed states as

$$[N_m''(t)]^2=2[1+(-1)^m e^{-r_0^2/2}]\ . \tag{64}$$

Each of the squeezed state components of this Schrödinger "cat" has a squeezing of

$$s'=\tfrac{1}{2}\ln\left[\frac{1+e^{2s(t)}}{2}\right]. \tag{65}$$

This approximation to the state reveals it to be a special kind of Schrödinger "cat." Two examples of the exact and approximate photon number distributions are illustrated in Fig. 14. It is interesting to note that a better approximation is found by using Stirling's formula on Eq. (50), but this does not offer an obvious interpretation.

In Fig. 11 the solid curve shows the quantum jumps of an initial squeezed vacuum. Unlike the case of the Schrödinger "cat" (the even and odd coherent states) we find that there are more than two trajectories present. This is because at each jump the state vector becomes increasingly complicated and the approximate state vector (63) comprises two Schrödinger "cat" components with a separation that depends on the number of jumps m through Eq. (60). However, there are two families of trajectories reflected in the change of sign in Eq. (63) and in the fact that the state vector contains only even Fock states for even m and only odd Fock states for odd m. In the latter case the mean photon number always ap-

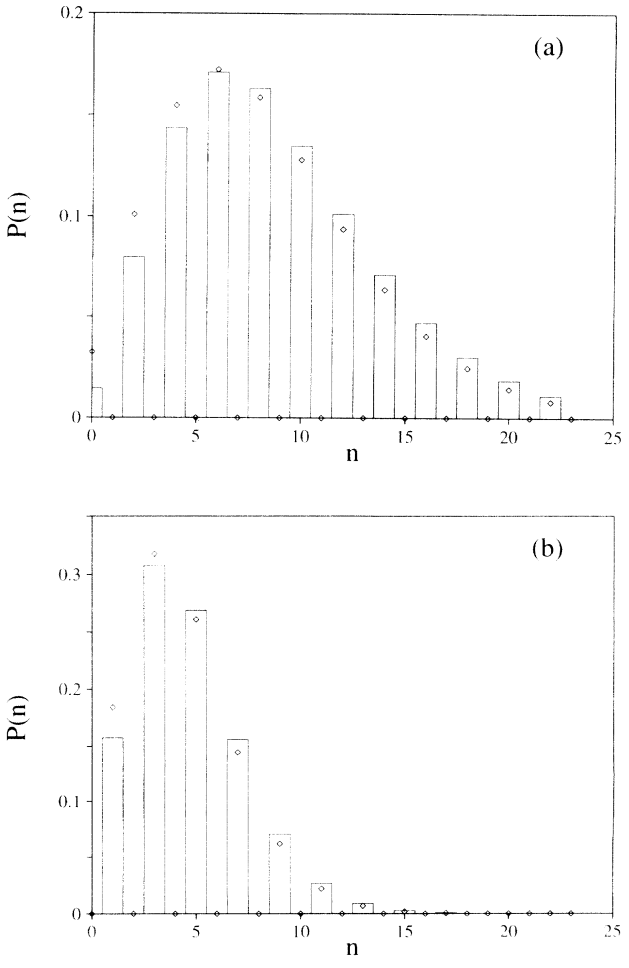


FIG. 14. The exact (solid line) and approximate (diamonds) photon-number distributions of the state (49) for (a) $s=0.8$ and $m=4$ and (b) $s=0.4$ and $m=7$. The results are from Eq. (50) and the Fock state expansion of Eq. (63).

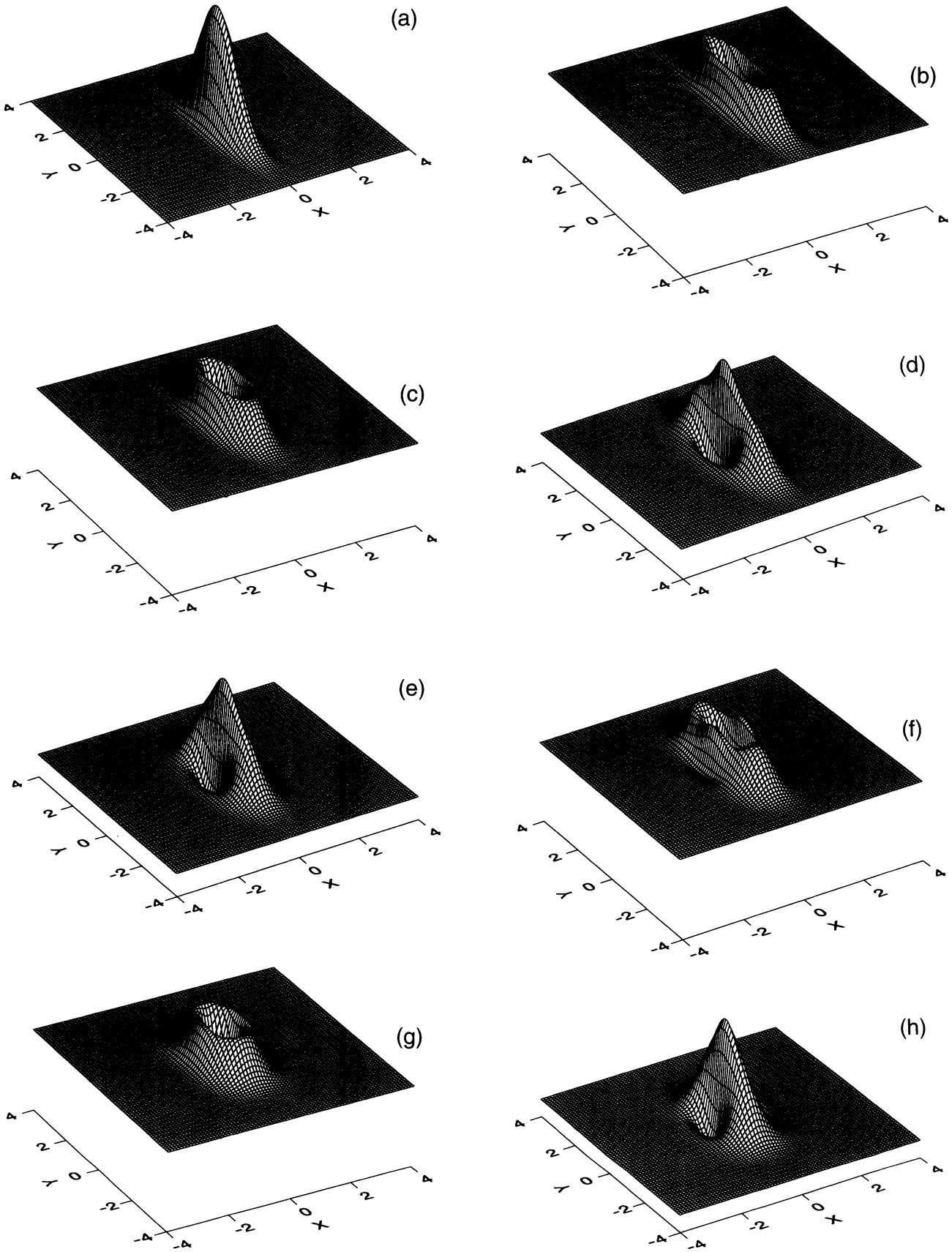


FIG. 15. The Wigner functions of the quantum state as it evolves through the first four quantum jumps seen in Figs. 11 and 12. The Wigner functions shown are (a) before and (b) after the quantum jumps at $\kappa t = 0.079$, (c) before and (d) after the quantum jump at $\kappa t = 0.350$, (e) before and (f) after the quantum jump at $\kappa t = 0.574$, and (g) before and (h) after the quantum jump at $\kappa t = 1.339$

proaches one for large κt, although for large enough κt there is at least one more jump to come. The fluctuations are shown in Fig. 12 and exhibit a character that is similar to the even and odd coherent states of Fig 2. However, there is a much greater degree of squeezing in Fig. 12. This can be understood from the approximate solution (63) because the direction of the squeezing of the "cat" components in phase space is at right angles to the direction along which they are aligned. This is more clearly seen from the plots of the Wigner function shown in Fig. 15. The initial Wigner function has been seen in the quantum-state diffusion case in Fig. 10(a) and is clearly squeezed in the x direction. Figure 15(a) shows the evolution under H_{eff} up to the point of a jump; consequently there has only been a reduction in the squeezing according to Eq. (47). After the first quantum jump in Fig. 15(b) a hole is forming in the center of the Wigner function. Evolution without jumps continues in Fig. 15(c) with a further loss of squeezing. The second jump in Fig. 15(d) results in a return to squeezing in ΔX and a Wigner function that looks remarkably like that of the even coherent state. This evolves in Fig. 15(e) and jumps in Fig. 15(f), resulting in a Wigner function similar to that of the odd coherent state. However, we know from Eq. (63) that it is better approximated by the superposition of squeezed states given there. After a much greater elapse of time [Figs. 15(g) and 15(h)], the Wigner function lacks a close resemblance to that of a Schrödinger "cat" because so few photons are left.

V. CONCLUSION

A quantum state in phase space is described by a patch (or patches) whose center dictates mean values and whose extent dictates the size of the fluctuations. Different representations of the patch in terms of various basis states result in different "tilings" of phase space: for an oscillator, energy eigenstates containing specific quanta are essentially annuli with zero mean amplitude, whereas coherent states tile phase space with circles each centered on a specific mean amplitude. Individual realizations are conditioned by the specific information gained by the measurement scheme. The two simulation schemes examined here reflect different kinds of conditioning and emphasize their own preferred phase-space tiling as we have shown. We have illustrated these preferences with a number of nonclassical superposition states. The localization phenomenon has been exhibited for an initial Schrödinger "cat," Fock state, and the squeezed vacuum, with the use of the Wigner phase-space quasiprobability. We have presented analytic results for arbitrary initial states after a finite number of quantum jumps, leading to the "jumping cat" in the case of an initial superposition of two coherent states. For the squeezed vacuum we have shown how the detection of photons results in the emergence of a special Schrödinger "cat" with squeezed state components.

ACKNOWLEDGMENTS

This work was supported in part by the United Kingdom Science and Engineering Research Council and by the European Community.

[1] B. W. Shore and P. L. Knight, J. Mod. Opt. **40**, 1195 (1993), and references therein.
[2] M. Sargent III, M. O. Scully, and W. Lamb, Jr., *Laser Physics* (Addison, Wesley, Rading, MA, 1974).
[3] W. H. Louisell, *Quantum Statistical Properties of Radiation* (Wiley, New York, 1973).
[4] J. P. Paz, S. Habib, and W. H. Zurek, Phys. Rev. D **47**, 488 (1993); W. H. Zurek, Phys. Today **44** (10), 36 (1991); **46**, 84 (1993); W. H. Zurek, Prog. Theor. Phys. **89**, 281 (1993); W. H. Zurek, S. Habib, and J. P. Paz, Phys. Rev. Lett. **70**, 1187 (1993), and references therein.
[5] E. Joos and H. D. Zeh, Z. Phys. B **59**, 223 (1985); D. F. Walls and G. J. Milburn, Phys. Rev. A **31**, 2403 (1985); S. J. D. Phoenix, *ibid.* **41**, 5132 (1990).
[6] G. J. Milburn, Phys. Rev. A **36**, 5271 (1987).
[7] Th. Sauter, W. Neuhauser, R. Blatt, and P. E. Toschek, Phys. Rev. Lett. **57**, 1696 (1986); J. C. Bergquist, R. G. Hulet, W. M. Itano, and D. J. Wineland, *ibid.* **57**, 1699 (1986); W. Nagourney, J. Sandberg, and H. Dehmelt, *ibid.* **56**, 2797 (1986); E. Peik, G. Hollemann, and H. Walther, Phys. Rev. A **49**, 402 (1994).
[8] N. Gisin, P. L. Knight, I. C. Percival, R. C. Thompson, and D. C. Wilson, J. Mod. Opt. **40**, 1663 (1993).
[9] M. Brune, S. Haroche, J. M. Raimond, L. Davidovich, and N. Zagury, Phys. Rev. A **45**, 5193 (1992).
[10] L. Davidovich, A. Maali, M. Brune, J. M. Raimond, and S. Haroche, Phys. Rev. Lett. **71**, 2360 (1993).
[11] G. Benson, G. Raithel, and H. Walther, Phys. Rev. Lett. **72**, 3506 (1994).
[12] H. J. Carmichael, *An Open Systems Approach to Quantum Optics*, Lecture Notes in Physics m18 (Springer-Verlag, Berlin, 1993).
[13] J. Dalibard, Y. Castin, and K. Mølmer, Phys. Rev. Lett. **68**, 580 (1992); K. Mølmer, Y. Castin, and J. Dalibard, J. Opt. Soc. Am. B **10**, 524 (1993).
[14] Y. Castin, J. Dalibard, and K. Mølmer, *Atomic Physics 13*, edited by H. Walther, T. W. Hänsch, and B. Neizert (AIP, New York, 1993), p. 143.
[15] N. Gisin and I. C. Percival, J. Phys. A **25**, 5677 (1992); **26**, 2233 (1993); **26**, 2245 (1993).
[16] T. P. Spiller, B. M. Garraway, and I. C. Percival, Phys. Lett. A **179**, 63 (1993).
[17] H. M. Wiseman and G. J. Milburn, Phys. Rev. A **47**, 642 (1993).
[18] N. Gisin and Y. Salama, Phys. Lett. A **181**, 269 (1993); N. Gisin, J. Mod. Opt. **40**, 2313 (1993).
[19] I. C. Percival, J. Phys. A **27**, 1003 (1994).
[20] G. C. Hegerfeldt and T. S. Wilser, in *II International*

Wigner Symposium, 1991 (World Scientific, Singapore, 1992); G. C. Hegerfeldt and M. B. Plenio (unpublished).
[21] C. Cohen-Tannoudji, B. Zambon, and E. Arimondo, J. Opt. Soc. Am. B **10**, 2107 (1993).
[22] P. Goetsch and R. Graham, Ann. Phys. (Leipzig) **2**, 706 (1993).
[23] B. M. Garraway and P. L. Knight, Phys. Rev. A **49**, 1266 (1994).
[24] B. M. Garraway, P. L. Knight, and J. Steinbach (unpublished).
[25] B. M. Garraway and P. L. Knight, in *Quantum Optics VI,* edited by J. D. Harvey and D. F. Walls (Springer-Verlag, Berlin, in press).
[26] A. Imamoğlu, Phys. Rev. A **48**, 770 (1993).
[27] W. G. Teich and G. Mahler, Phys. Rev. A **45**, 3300 (1992).
[28] L. Tian and H. J. Carmichael, Phys. Rev. A **46**, 6801 (1992).
[29] R. Dum, P. Zoller, and H. Ritsch, Phys. Rev. A **45**, 4879 (1992).
[30] C. W. Gardiner, A. S. Parkins, and P. Zoller, Phys. Rev. A **46**, 4363 (1992).
[31] R. Dum, A. S. Parkins, P. Zoller, and C. W. Gardiner, Phys. Rev. A **46**, 4382 (1992).
[32] M. J. Holland, K.-A. Suominen, and K. Burnett, Phys. Rev. Lett. **72**, 2367 (1994); M. J. Holland, D.Phil. thesis, University of Oxford, 1994.
[33] W. K. Lai, K.-A. Suominen, B. M. Garraway, and S. Stenholm, Phys. Rev. A **47**, 4779 (1993).
[34] W. K. Lai and S. Stenholm, Opt. Commun. **104**, 313 (1994).
[35] G. Lindblad, Commun. Math. Phys. **48**, 119 (1976).
[36] H. M. Wiseman and G. J. Milburn, Phys. Rev. A **47**, 1652 (1993); also I. C. Percival (unpublished).
[37] K. Mølmer (unpublished).
[38] G. J. Milburn, Phys. Rev. A **44**, 5401 (1991).
[39] H. Moya-Cessa, V. Bužek, M. S. Kim, and P. L. Knight, Phys. Rev. A **48**, 3900 (1993).
[40] N. Gisin, Phys. Rev. Lett. **52**, 1657 (1984); N. Gisin, Helv. Phys. Acta **62**, 363 (1989); L. Diósi, J. Phys. A **21**, 2885 (1988); Phys. Lett. A **129**, 419 (1988); P. Pearle, Phys. Rev. A **39**, 2277 (1989); G. C. Chirardi, P. Pearle, and A. Rimini, *ibid.* **42**, 78 (1990); N. Gisin and I. C. Percival, Phys. Lett. A **167**, 315 (1992).
[41] R. Loudon, *Quantum Theory of Light,* 1st ed. (Oxford University Press, Oxford, 1973).
[42] See, for example, C. W. Gardiner, *Quantum Noise* (Springer-Verlag, Berlin, 1991).
[43] H. J. Carmichael, S. Singh, R. Vyas, and P. R. Rice, Phys. Rev. A **39**, 1200 (1989).
[44] M. D. Srinivas and E. B. Davies, Opt. Acta **28**, 981 (1981); M. Ueda, Phys. Rev. A **41**, 3875 (1990); M. Ueda, N. Imoto, and T. Ogawa, *ibid.* **41**, 3891 (1990); M. Ueda and M. Kitagawa, Phys. Rev. Lett. **68**, 3424 (1992).
[45] N. Lu, Phys. Rev. A **40**, 1707 (1989); S. M. Barnett and P. L. Knight, *ibid.* **33**, 2444 (1986).
[46] J. Peřina, *Quantum Statistics of Linear and Nonlinear Optical Phenomena* (Reidel, Dordrecht, 1984).
[47] U. M. Titulaer and R. J. Glauber, Phys. Rev. **145**, 1041 (1966); D. Stoler, Phys. Rev. D **4**, 2309 (1971); Z. Bialynicka-Birula, Phys. Rev. **173**, 1207 (1968).
[48] K. Vogel and H. Risken, Phys. Rev. A **40**, 2847 (1989); D. T. Smithey, M. Beck, M. G. Raymer, and A. Faridani, Phys. Rev. Lett. **70**, 1244 (1993).
[49] B. M. Garraway and P. L. Knight, Phys. Rev. A **46**, 5346 (1992).
[50] V. Bužek, A. Vidiella-Barranco, and P. L. Knight, Phys. Rev. A **45**, 6570 (1992).
[51] P. Adam, J. Janszky, and A. V. Vinogradov, Opt. Commun. **80**, 155 (1990); see also C. W. Gardiner, *Quantum Noise* (Springer-Verlag, Berlin, 1991); V. Bužek and P. L. Knight, Opt. Commun. **81**, 331 (1991); V. Bužek and P. L. Knight, in *Progress in Optics,* edited by E. Wolf (North-Holland, Amsterdam, in press).
[52] R. Loudon and P. L. Knight, J. Mod. Opt. **34**, 709 (1987), and references therein.
[53] T. Ogawa, M. Ueda, and N. Imoto, Phys. Rev. A **43**, 6458 (1991).
[54] R. Gilmore, J. Math. Phys. **15**, 2090 (1974).
[55] H. P. Yuen, Phys. Rev. A **13**, 2226 (1976).
[56] P. Adam, I. Földesi, and J. Janszky, Phys. Rev. A **49**, 1281 (1994).

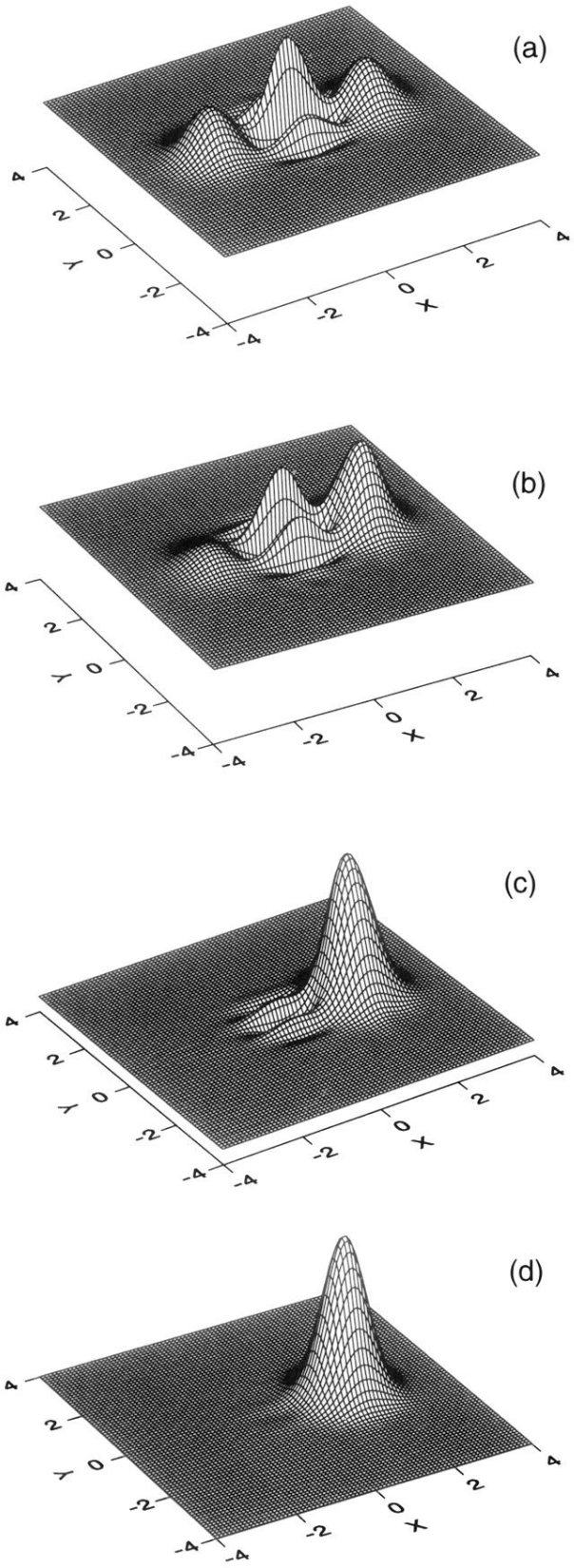


FIG. 1. Localization of a Schrödinger "cat" state which is initially the even coherent state $|2.0,+\rangle$ as defined in Eq. (26). These results are an example of a single sample undergoing quantum-state diffusion. We depict the Wigner functions for $\kappa t = 0$, 0.1, 0.2, and 0.5 in (a)–(d). Localization is seen as the increasing dominance of one component of the "cat."

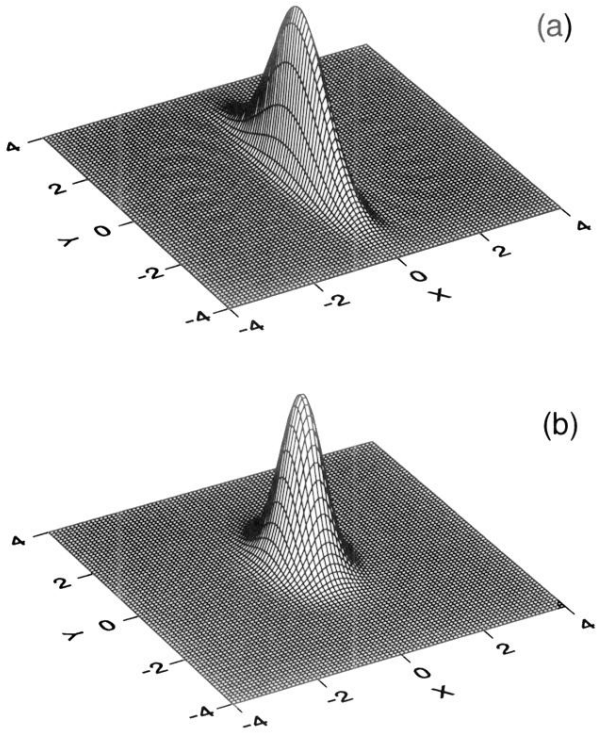


FIG. 10. Wigner functions in a quantum-state diffusion simulation starting from a squeezed vacuum state [Eq. (33)] with $s(0)=0.8$ and $\theta=0$. In (a) we show the initial state and in (b) we show the Wigner function when $\kappa t=1.0$. In the latter case the Wigner function has lost much of its squeezing, but is displaced from the phase-space origin.

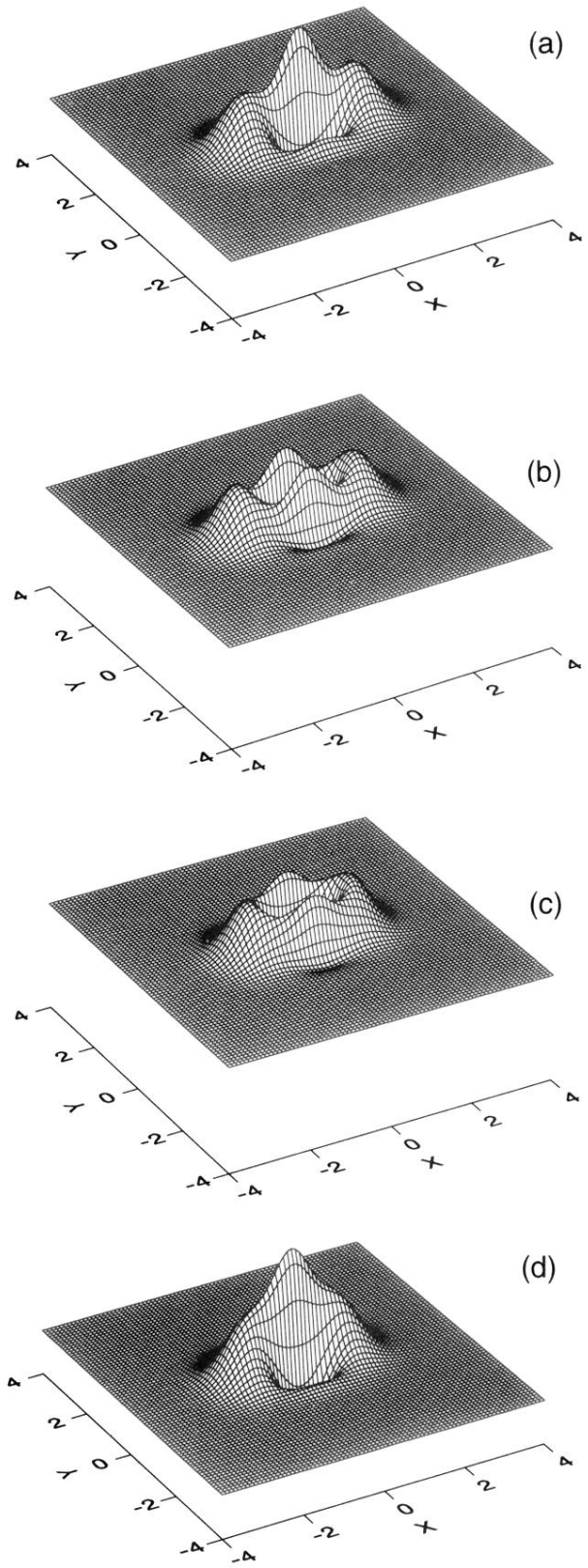


FIG. 13. A "jumping cat" that was initially comprised of the coherent states $|\alpha\rangle$ and $|-\alpha\rangle$ with $\alpha=2$. These results are for a single sample where the internal phase of the cat changes at each quantum jump. We show the Wigner functions before and after the first jump (at $\kappa t=0.708$) in (a) and (b). In (c) and (d) we show the Wigner functions before and after the second jump (at $\kappa t=1.127$). The same jumps are seen in Figs. 2–4.

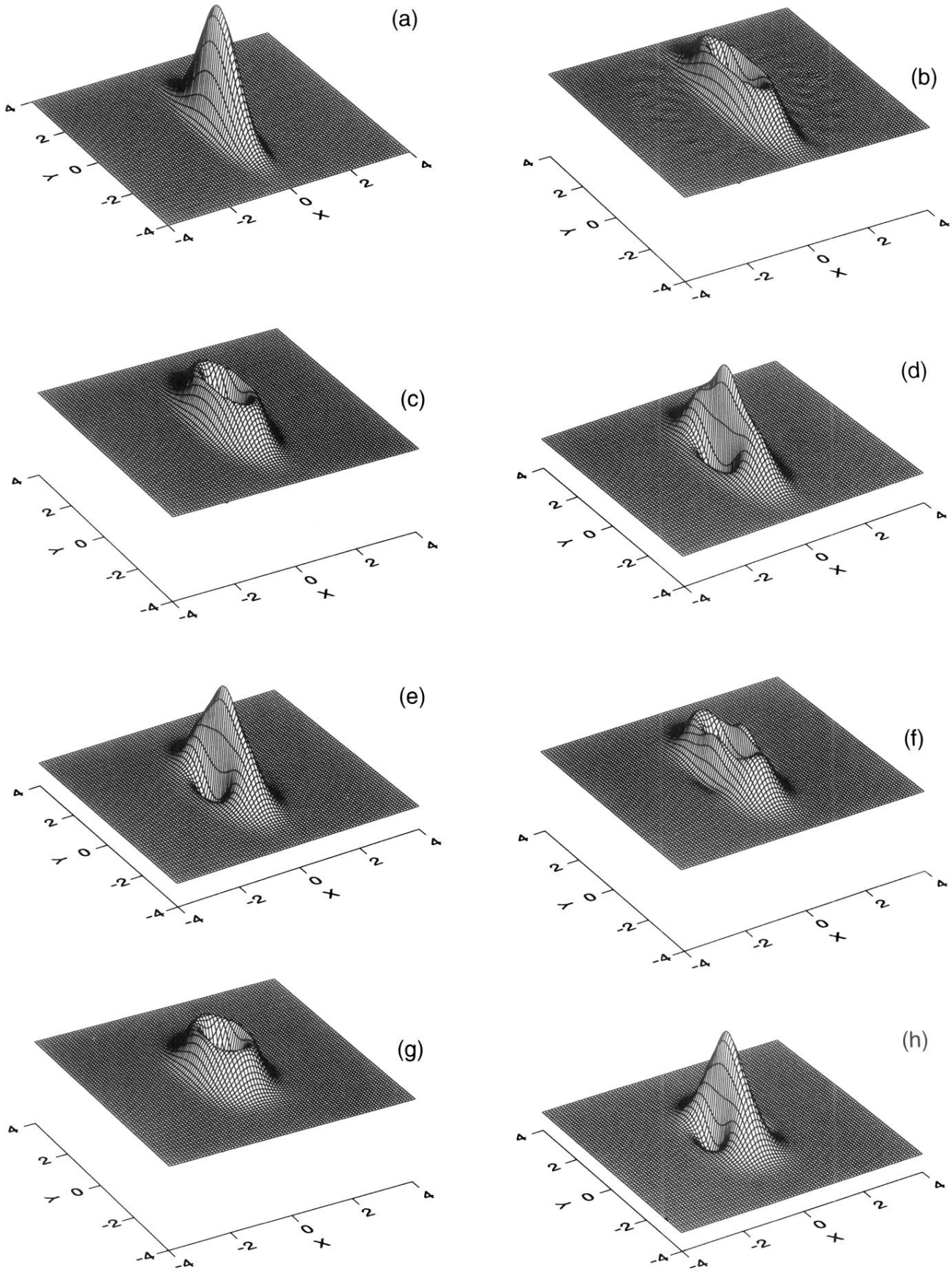


FIG. 15. The Wigner functions of the quantum state as it evolves through the first four quantum jumps seen in Figs. 11 and 12. The Wigner functions shown are (a) before and (b) after the quantum jumps at $\kappa t = 0.079$, (c) before and (d) after the quantum jump at $\kappa t = 0.350$, (e) before and (f) after the quantum jump at $\kappa t = 0.574$, and (g) before and (h) after the quantum jump at $\kappa t = 1.339$

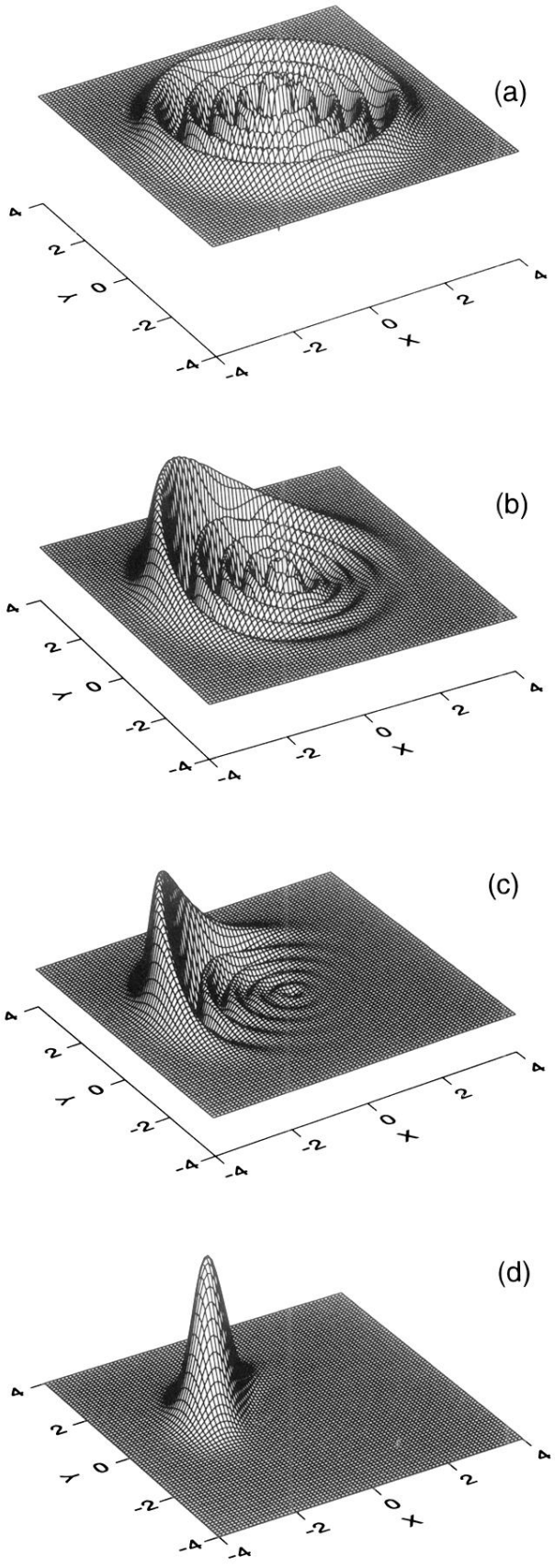


FIG. 5. Localization of a Fock state with $n=9$. These results are for a single sample undergoing quantum-state diffusion. The Wigner functions are shown for $\kappa t=0$, 0.1 0.2, and 1.0 in (a)–(d).